

See discussions, stats, and author profiles for this publication at: <https://www.researchgate.net/publication/230582476>

Investigation of Gas Permeability in Carbon Nanotube (CNT)-Polymer Matrix Membranes via Modifying CNTs with Functional Groups/Metals and Controlling Modification Location

ARTICLE *in* THE JOURNAL OF PHYSICAL CHEMISTRY C · APRIL 2011

Impact Factor: 4.77 · DOI: 10.1021/jp1120965

CITATIONS

20

READS

93

7 AUTHORS, INCLUDING:



Lei Ge

eResearch Australasia - University of Queens...

47 PUBLICATIONS 1,187 CITATIONS

[SEE PROFILE](#)



Feng Li

Chinese Academy of Sciences

213 PUBLICATIONS 14,111 CITATIONS

[SEE PROFILE](#)



Lianzhou Wang

University of Queensland

218 PUBLICATIONS 5,532 CITATIONS

[SEE PROFILE](#)



Xue-Gang Tang

University of Queensland

21 PUBLICATIONS 163 CITATIONS

[SEE PROFILE](#)

Investigation of Gas Permeability in Carbon Nanotube (CNT)–Polymer Matrix Membranes via Modifying CNTs with Functional Groups/Metals and Controlling Modification Location

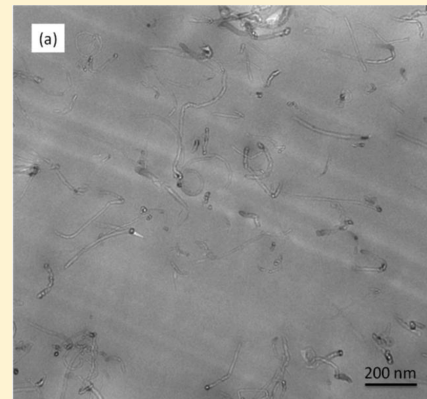
Lei Ge,[†] Zhonghua Zhu,^{*,†} Feng Li,[‡] Shaomin Liu,[§] Li Wang,[†] Xuegang Tang,[†] and Victor Rudolph[†]

[†]School of Chemical Engineering, and [‡]School of Mechanical Engineering, The University of Queensland, Brisbane 4072, Australia

[§]School of Physics, Taishan University, Shandong, China

[§]School of Chemical Engineering, Curtin University of Technology, Perth, Australia

ABSTRACT: Metal- or functional group-modified multiwalled carbon nanotubes (CNTs) were embedded into the poly(ether sulfone) (PES) polymer matrix to study the gas permeability of the nanocomposite membranes. Carboxyl-functionalized CNTs and Ru (Fe) metal-modified CNTs were prepared via acid oxidation and wet impregnation methods, respectively. The derived nanocomposite membranes show similar crystalline structure and CNT dispersion as well as improvement in gas permeation fluxes at low CNT concentration (<5 wt %). However, the CO₂/N₂ selectivity varies with different modification components. Compared with pure polymer membranes, those containing Ru-modified CNTs show higher gas selectivity, while Fe-modified CNT membranes show lower selectivity, and carboxyl CNT composite membranes are similar to pure PES membrane. By controlling Ru modification into CNT channels, poor gas selectivity of the corresponding membranes is observed. These results, combined with the results of density functional theory calculations, indicate that different gas adsorption behaviors are introduced via modification by metals or carboxyl functional groups and further influence the gas permeability. Based on both experimental and theoretical results, gas diffusion appears to pass through the interface between polymer chains and carbon nanotubes, rather than the CNT channels, in this nanocomposite system. Thereby, tailoring modification on the external surface of carbon nanotubes can be more effective for improving gas separation performance of CNT-based nanocomposite membranes.



1. INTRODUCTION

Polymeric membranes with advantages in effective operation, environmental benignity, and energy savings have been widely used in many areas, such as gas and vapor separation,^{1–3} water purification,⁴ sensor,⁵ and fuel cells.⁶ For all these applications, the ideal membrane should possess excellent stability under a wide range of process conditions, as well as a high selectivity and a large flux with a small driving force. However, most of the polymer membranes show trade-off properties because optimal mass transport rates and separation efficiency are difficult to achieve at the same time,^{7,8} and thus extensive industrial scale applications of such membranes have not occurred yet. Researchers have paid special attention to the relationship between polymer structure and gas separation properties in order to improve membrane separation performance.

The permeability of a dense polymer membrane is mainly controlled by the chain mobility, the packing density, and the free volume of the polymer structure. The introduction of a bulky substituent can be one of the best techniques to improve gas permeability by inhibiting molecular chain packing and increasing free volume. Therefore, polymer–inorganic nanocomposite membranes derived from the dispersal of inorganic nanofillers

into a polymer matrix at a nanometer level have been developed as an alternative approach to solve the trade-off problem of polymeric membranes.⁹ Compared to pure polymer membranes, many polymer–inorganic (such as silica and TiO₂) nanocomposite membranes show higher permeabilities without sacrificing gas selectivity, or even with improved selectivity.^{10–22} Among them, carbon nanotube (CNT)-based nanocomposite membranes have been developed for some time due to super high flux of gas diffusion in CNT tunnels as well as their enhanced tensile modulus and break stress.^{23–25} Molecular dynamics simulations predicted that the transport of light gases inside CNTs should be orders of magnitude faster than in any other known material, in fact as fast as in gases,^{26–28} due to the inherent smoothness of the nanotube. Experimental studies confirmed that carbon nanotubes, as the inorganic nanofillers in nanocomposite membranes, did facilitate gas permeability compared to the pure polymeric counterparts. For instance, Kim et al.²⁹ reported that the addition of CNTs to poly(imide siloxane)

Received: December 21, 2010

Revised: March 8, 2011

Published: March 23, 2011

membranes could increase the permeability of O₂, N₂, and CH₄ by 10–50%, however, accompanied with a unfortunate gas selectivity decrease. Cong et al.³⁰ also prepared the CNT-brominated poly(2,6-diphenyl-1,4-phenylene oxide) composite membrane with single-walled CNTs or multiwalled CNTs and found that low concentration of CNTs could increase the gas permeability without sacrificing selectivity. Multiwalled CNT/PBNPI membranes fabricated by Weng et al.³¹ showed improved permeability and the selectivity of H₂, CO₂, and CH₄ at high CNT concentrations (>5 wt %). Though different selectivity trends have been reported, the common view is that the interaction between polymer-chain segments and nanotubes disrupts the polymer-chain packing to create more voids (free volumes between the polymer chains and polymer/nanofiller interfaces), thus enhancing gas diffusion. The solubility is influenced by the interaction between permeates and the functional molecules on CNTs.^{32,33} However, the performances of these CNT-based nanocomposite membranes are not enhanced much; the selectivity shows a larger variation than the permeability. The detailed gas transport mechanism through the CNT–polymer composite membrane is still unclear. To understand the gas diffusion in CNT channels and the nanovoids between CNTs and polymer is important as this may provide theoretical guidance to design new composite membranes with improved permeability and selectivity.

It has been recognized that functional groups and metal nanoparticles on the surface of the inorganic nanofiller phase may interact with polar gases, such as CO₂ and SO₂, and increase the penetrant solubility in the nanocomposite membranes.³² For instance, higher CO₂ permeability and CO₂/N₂ selectivity was observed on the PEBAK/silica nanocomposite membranes,¹⁵ which was attributed to the strong interaction between CO₂ molecules and the residual hydroxyl groups on the silica, as well as the additional sorption sites in the polyamide block of PEBAK. In TiO₂–6FPAI nanocomposite membranes, the gas permeability increased due to the decreased sorption enthalpy caused by a strong interaction between CO₂ and TiO₂ domains.¹¹

Some simulation work on functionalization of carbon nanotubes with metal atoms also showed that the electronic structure of the CNT surface was greatly modified, which enhanced the gas adsorption (through interaction between the gas and the functional groups) inside the CNT, and the selectivity can be improved without sacrificing flux.^{34,35} Therefore, in this work, a series of poly(ether sulfone) nanocomposite membranes based on different modified CNTs were prepared and comparatively studied. The effect of modification component of CNTs on gas permeation behavior was investigated by first functionalizing CNTs with carboxyl groups or ruthenium or iron particles, then fabricating the corresponding membranes, and comparing their gas separation performance. For a more in-depth understanding of the gas diffusion behavior through the membranes, a molecular simulation was carried out to study the adsorption energy difference generated by different CNT functionalizations.

2. THEORY

Adding impermeable inorganic nanoparticles to a polymer is typically expected to reduce the gas permeability.³⁶ Maxwell's model is developed to analyze the steady-state dielectric

properties of a diluted suspension of spheres³⁷ and often used to model permeability in membranes filled with roughly spherical particles

$$P = P_p \left[\frac{1 - \Phi_f}{1 + 0.5\Phi_f} \right] \quad (1)$$

where P and P_p are the permeability of the nanocomposite and the pure polymer matrix, respectively, and Φ_f is the volume fraction of the nanofiller.

The second generalized Maxwell model³⁸ is used to estimate the permeation through a structured biphasic material wherein the additive component is randomly dispersed with sharp interfaces in a continuous matrix of the polymer, expressed as

$$P = P_p \left[1 + \frac{(1+G)\Phi_f}{\frac{P_f}{P_p} + G} \left(\frac{\frac{P_p}{P_f}}{\frac{P_p}{P_f} - 1} - \Phi_f \right) \right] \quad (2)$$

where P_f is the gas permeability in the CNT and G is a geometric factor accounting for dispersion shape. Based on molecular dynamics simulation results, the transport of light gases inside CNTs are orders of magnitude faster than in microporous materials, and much faster than in the glassy poly(ether sulfone) used in this manuscript. Taking the CO₂ permeation flux as the standard, gas flux through the aligned CNT membranes can reach 0.2×10^{-3} mol/m² s Pa³⁹ compared with $\sim 0.94 \times 10^{-15}$ mol/m² s Pa in poly(ether sulfone) membranes.⁴⁰ Therefore, the P_f/P_p value is nearly 2×10^{11} , and the equation can be simplified as

$$P = P_p \left[1 + \frac{(1+G)\Phi_f}{1 - \Phi_f + \frac{G}{2 \times 10^{11}}} \right] \quad (3)$$

If the dispersed phase is oriented in lamellae parallel to the direction of permeation, G tends to infinity, and there is minimum resistance to flow. If the disperse phase is oriented in lamellae perpendicular to the direction of permeation, G tends to zero, and maximum impedance of flow occurs due to obstructive layers of the less permeable component.

In this work, the CNTs volume fraction in PES has been estimated using the equation

$$\Phi_f = \frac{w_f}{w_f} + \frac{\rho_f}{\rho_p} (1 - w_f) \quad (4)$$

where ρ_p and ρ_f are the density of the pure PES polymer and CNTs, respectively, and w_f is the CNT weight fraction in the polymer.

3. EXPERIMENTAL SECTION

3.1. Materials. Poly(ether sulfone) (PES) was purchased from Radel A-300, Solvay Advanced Polymers. The multiwalled CNTs, produced from methane decomposition over Fe catalysts in a fluidized-bed reactor, were supplied by Tsinghua University, China, and the purity in the pristine samples was above 95%. The

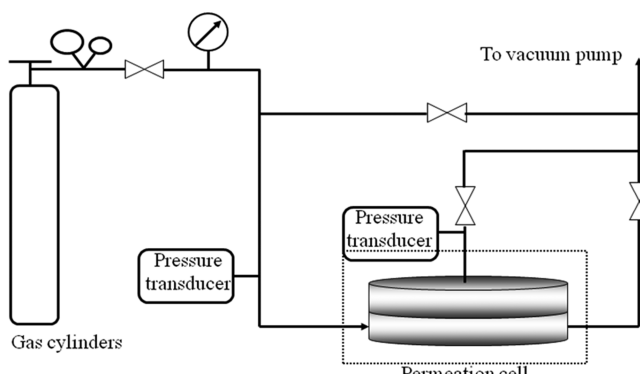


Figure 1. Diagram of the setup for the permeation measurement.

orientation of the carbon layers in a typical CNT is parallel to its axis. The external diameter of CNTs is in the range of 10–30 nm, and most CNTs have a diameter around 20 nm. The inner diameters are typically about one-third of the corresponding external diameters. Analytical grade *N*-methyl-2-pyrrolidone (NMP), sulfuric acid, nitric acid, iron nitrate, and ruthenium chloride were supplied by Sigma-Aldrich.

3.2. Multiwalled CNTs Functionalization. Carboxyl-modified CNTs were prepared according to the reported method.⁴¹ A 0.5 g amount of CNTs was sonicated in 300 mL of a mixture of concentrated H₂SO₄ (98 vol %)/HNO₃ (70%) (3:1) for 3 h at 60 °C. Then the sample was washed with deionized water by several centrifugation/redisersion cycles and filtered with a 0.2 μm pore size membrane filter, followed by drying under vacuum. Finally, well-dispersed CNTs were obtained with oxidized carboxylic groups on the outer walls as previously reported.^{42,43}

Ru- and Fe-functionalized multiwalled carbon nanotubes were prepared by the wet impregnation method using the acetone solution of RuCl₃ and Fe(NO₃)₃, respectively. The carbon nanotubes were purified with 5 M HNO₃ at 110 °C for 5 h to remove amorphous carbon and residual Fe catalyst before metal loading. The loading contents of both metals on purified CNTs were fixed at 5 wt %. The samples were then dried at 110 °C for 5 h and calcined at 500 °C under the protection of ultrahigh purity argon gas. The reduction was carried out at 500–650 °C in Ar/H₂ atmosphere for 3–5 h and then cooled to room temperature in Ar. The samples were labeled as COOH-CNT, Ru-CNT, and Fe-CNT for carboxyl-, Ru-, and Fe-modified CNTs, respectively. The Ru and Fe metal particles are mainly on the external surface of the close-ended carbon nanotubes.

To selectively deposit Ru nanoparticles into the CNT nanochannels, catalytic oxidation was used to open the tube ends, followed by a Ru incipient impregnation method. The catalytic oxidation of CNTs with a Ag catalyst followed the method described by Wang et al.⁴⁴ First, CNTs were impregnated with 5 wt % Ag from a 0.005 M solution of AgNO₃. The solution was stirred at 40 °C until almost dry and then dried completely in an oven at 100 °C. The AgNO₃/CNTs were heated at 3 °C/min to 300 °C under Ar and held at 300 °C for 3 h to decompose AgNO₃ to Ag. Catalytic oxidation was performed under Ar in a tube furnace with Ag/CNTs placed in a quartz boat and heated at 3 °C/min to 350 °C. When the furnace temperature stabilized at 350 °C, the gas was switched from Ar to 5 vol % O₂ in He (50 mL/min) for 60–90 min. Oxidized Ag/CNTs were sonicated in 2 M nitric acid and washed with deionized water to remove the Ag nanoparticles. The incipient impregnation process was the same

as the outer surface modification as above. The product was labeled as Ru-in-CNT for comparison.

3.3. Membrane Preparation. The dense pure PES membrane or carbon nanotubes/poly(ether sulfone) (CNTs-PES) composite membranes were fabricated by phase transition method followed by compression molding. The preparation of CNTs-PES membranes was as follows: first, the specific percentage of modified CNTs was added in *N*-methyl-2-pyrrolidone (NMP) solvent and dispersed by sonication for several hours to enhance the homogeneity. Then the PES/NMP mixture solution (weight ratio = 1:4) was added to the slurry and stirred at high velocity for 12–36 h to disperse CNTs uniformly in the polymer matrix. The concentration of CNTs was 0–10 wt % in this study. The mixture was then cast onto clean and dry glass plates at room temperature. The nascent membranes were immersed into a water bath for 24 h, followed by drying in a vacuum oven at 170 °C for 1–2 days. The thickness of the dense membranes was controlled by compression molding (270 °C and 5.0 MPa) to 30–50 μm for subsequent characterization.

3.4. Characterization. The X-ray diffraction spectra (XRD) of PES and nanocomposite membranes were obtained with a Bruker Advanced X-ray Diffractometer (40 kV, 30 mA) with Cu Kα ($\lambda = 0.154\text{06 nm}$) radiation at a scanning rate of 1°/min from 5° to 90°. The ultrathin TEM nanocomposite samples (about 50–100 nm in thickness) were cut on a Leica EM UC6 ultra microtome (Leica Microsystems, Wetzlar, Germany) and then investigated using a JEOL TEM 1010 equipped with field emission gun (FEG) at 100 kV. Digital images were acquired by a Gatan CCD camera. The thermal properties of pure PES and CNTs-PES membranes were measured by means of a TA Q20 differential scanning calorimeter in nitrogen atmosphere. The samples were initially heated from 50 to 320 °C, cooled with liquid nitrogen, held for 5 min, and processed two more times following the same steps, under nitrogen atmosphere, with a heating rate as 10 °C/min and the cooling rate as 20 °C/min. The glass transition temperature, T_g , of the polymer was obtained from the third scan. X-ray photoelectron spectroscopy (XPS) was performed on a PHI-560 ESCA (Perkin-Elmer) using a nonmonochromatic Mg Kα excitation source at 15 kV. The C1s peak position was set to 284.6 eV and taken as an internal standard. Quantitative analysis was performed with CASAXPS software after Shirley background subtraction. The best fit peaks were obtained using mixed 30% Gaussian–Lorentzian line shapes.

3.5. Permeation Test. The variable feed pressure and the constant volume permeation system were used to test pure-gas permeation fluxes at room temperature, with the permeation apparatus shown in Figure 1. The membranes were held under vacuum for approximately 5 min to achieve a steady state before the exposing to the selected gas at a specific pressure.

The permeation coefficient is calculated using the following equation

$$P = \frac{273.15 \times 10^{10}}{760AT} \frac{VL}{P_0 \times 76} \frac{dp}{dt} \quad (5)$$

14.7

where P is the permeation coefficient in barrer (1 barrer = $1 \times 10^{-10} \text{ cm}^3 (\text{STP}) \text{ cm cm}^{-2} \text{ s}^{-1} \text{ cm Hg}^{-1}$), A is the effective area of the membrane (cm²), T is the absolute temperature (K), V is the dead-volume of the downstream chamber (cm³), L is the membrane thickness (cm), P_0 is the feed pressure (psi), and

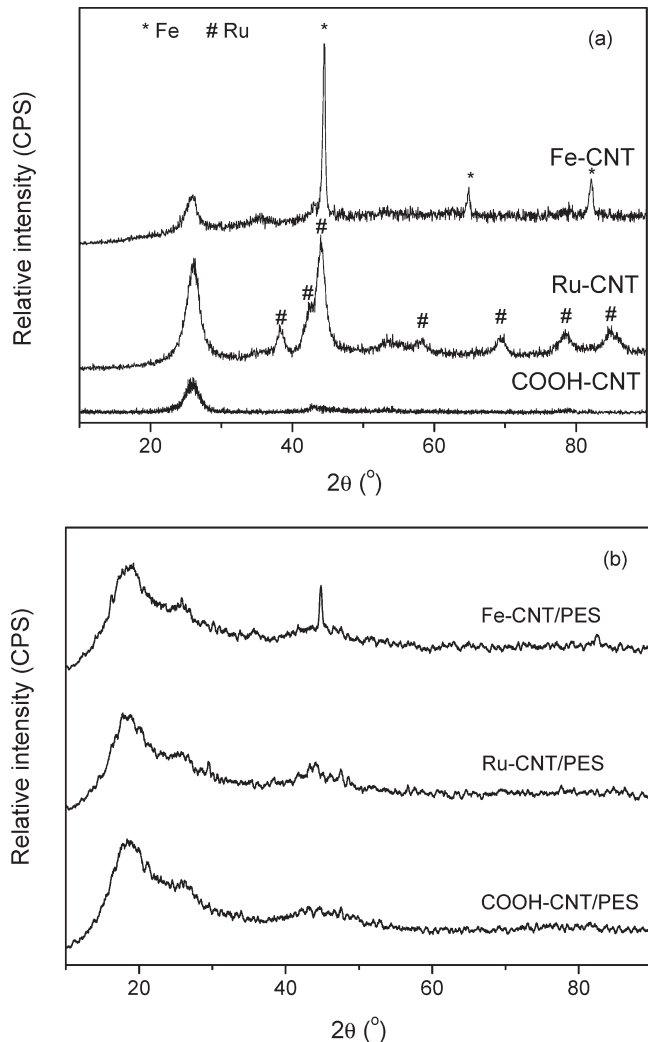


Figure 2. XRD patterns of 10 wt % of the modified CNTs (a) and corresponding nanocomposite membranes (b).

dP/dt is the steady rate of pressure increase in the downstream side (mm Hg s^{-1}). Values and error bars reported in the tables and figures are based on measurements of three different membrane samples.

The ideal selectivity for two gases is determined as

$$\alpha = \frac{P_A}{P_B} \quad (6)$$

where P_A and P_B are the permeation coefficients of pure gas A and B, respectively.

3.6. Computational Details. To understand the different adsorption behaviors of gas molecules on the metal- or functional groups-modified CNTs, the adsorption configurations and energies of one gas molecule adsorbed on the inner or outer surface of the (6,6) CNT modified with one Ru, Fe, or COOH adsorbed on the external surface of the tube were calculated using density functional theory. The length of the supercell was 12.3 Å for the (6,6) CNT consisting of 120 C atoms. Periodic boundary conditions along the tube axis were employed, and a vacuum region (at least 16.0 Å) between CNTs was applied along the radial direction to decouple the interaction between adjacent tubes to ensure an isolated one-dimensional nanotube being

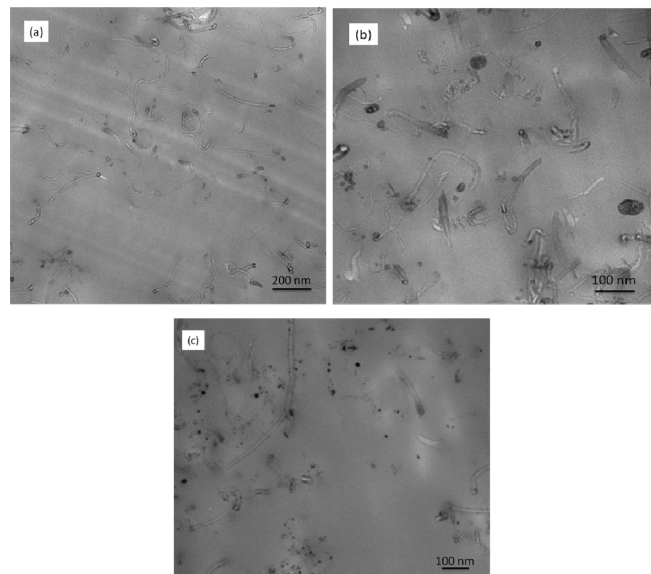


Figure 3. TEM images of 5 wt % modified CNTs in PES membranes: (a) COOH-CNT; (b) Fe-CNT; (c) Ru-CNT.

considered. All the calculations were performed using the Siesta package.^{45,46} The ion–electron interaction was modulated by ab initio norm-conserving fully separable Troullier–Martins⁴⁷ pseudopotential in Kleinman–Bylander form.⁴⁸ The exchange correlation potential was treated using the local density approach (LDA) in Perdew–Zunger parametrization.⁴⁹ The atomic orbital basis set employed throughout was a double- ζ plus polarization (DZP) orbital. The charge density was calculated in a regular real space grid with cutoff energy of 120 Ry. For sampling the Brillouin zone (BZ), a set of eight Monkhorst–Pack special k-points⁵⁰ was used along the tube axis. The adsorption energy, E_a , of a gas molecule adsorbed on the doped (6,6) CNT was calculated by the expression

$$E_a = E_{\text{tot(CO}_2/\text{N}_2)} + E_{\text{tot(CNT)}} - E_{\text{tot(CNT + N}_2/\text{CO}_2)} \quad (7)$$

where $E_{\text{tot(CO}_2/\text{N}_2)}$, $E_{\text{tot(CNT)}}$, and $E_{\text{tot(CNT+N}_2/\text{CO}_2)}$ are the total energies of a gas molecule (CO_2/N_2), the modified CNT, and the modified CNT with the gas molecule, respectively.

4. RESULTS AND DISCUSSION

4.1. Characterizations of Functionalized Carbon Nanotubes and Nanocomposite Membranes. Figure 2 shows the X-ray diffraction patterns of carboxyl-, Fe-, and Ru-modified CNTs (a) and the fabricated nanocomposite membranes (b). The carboxyl functional groups have little influence on the carbon nanotube X-ray diffraction pattern (002, 100, and 004), which only illustrates three crystalline peaks at $2\theta = 26^\circ$, 43° , and 54° of CNTs. The marked peaks in metal-modified CNT samples indicate that Ru and Fe are successfully incorporated into the CNTs, as also confirmed by TEM observations discussed in the subsequent section. In Figure 2a, Fe has a sharper XRD peak than Ru, indicating a larger Fe particle size than Ru. Apart from the property difference between Ru and Fe themselves, another reason is that Fe oxide needs a higher reduction temperature than Ru oxide. In our experiments, Fe-CNT was reduced at 650 °C while Ru-CNT was reduced at 500 °C.

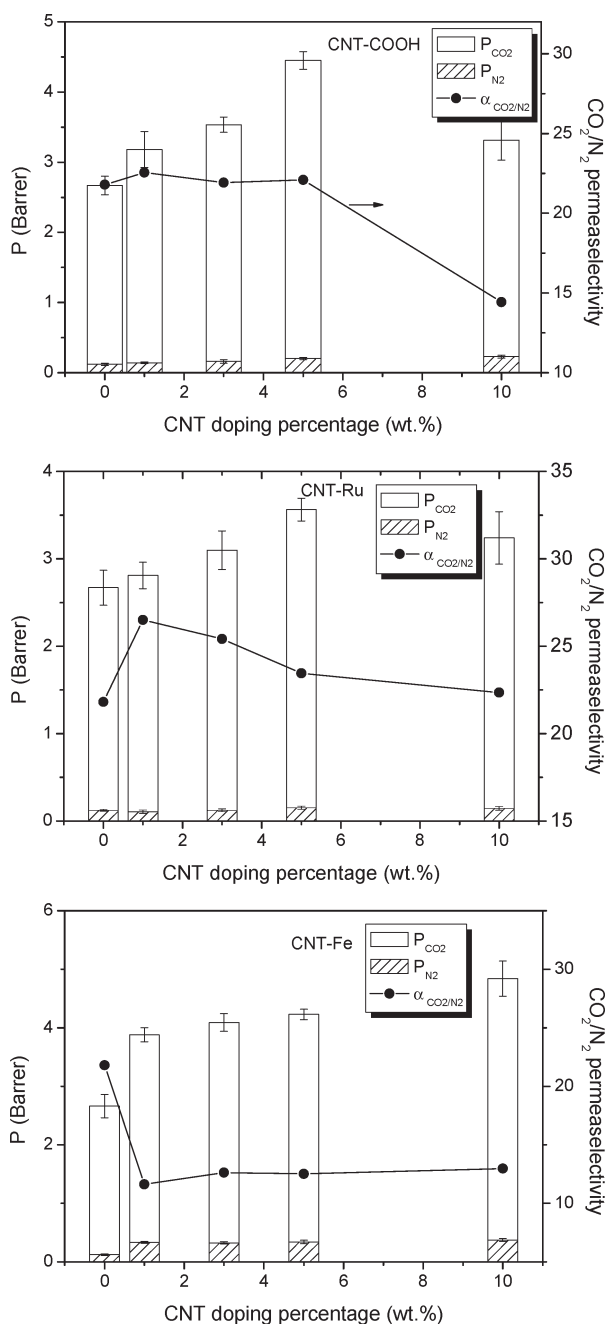


Figure 4. CO_2/N_2 separation performance of nanocomposite membranes as a function of CNTs concentration via modification (test conditions: 2 bar feed pressure gradient at 25 °C).

Crystallinity of polymers is one of the factors determining their transport properties. Gas permeation through the polymer membrane can occur in either amorphous material or interstices between crystallites.^{51,52} In Figure 2b, the broad peak at $2\theta = 18^\circ$ can be assigned to PES, a characteristic peak of the pure poly(ether sulfone) polymer.^{53,54} No significant change in the XRD patterns can be detected between pure PES membrane and the composite membranes (Figure 2b), except for the additional peaks assigned to the CNT phase ($2\theta = 26^\circ$) and modified components (Figure 2a). Even with the largest addition (10 wt %) of CNTs into the PES matrix, the nanocomposite membranes still possess the amorphous structure because the

phase of polymer matrix remains unchanged with the addition of CNTs.

Uniform dispersion of nanotubes or particles inside the polymer matrix is the prerequisite of successful application of nanocomposite membranes. More than 10 different positions on the thin films were observed at various magnifications by TEM. Representative images are shown in Figure 3. As can be seen, the nanocomposite membrane samples (a–c) still maintain the dense structure after the incorporation of carbon nanotubes, and no voids or pores can be observed in the film. Helium leaking test was also conducted and confirms that no through pores are formed during membrane preparation; thus, gas transportation through the nanocomposite membranes still follows the solution-diffusion model.

Examination of the TEM images reveals that most of the carbon nanotubes are well-dispersed in the polymer matrix without the presence of CNT agglomerates. The phase inversion process adopted in this study can generate fast desolvation and reduce the agglomeration possibility. Considering that such a uniform dispersion is difficult to achieve for pristine CNTs by simple mechanical mixing, the achievement of such nanoscale dispersion is not only related attributed to the well-controlled experimental procedure, but also to the good wetting property of the functionalized carbon nanotubes. Moreover, TEM images also indicate that the CNTs are randomly dispersed inside the polymer, and there remains an issue about how to postalign these CNTs in the polymer matrix in one radial direction parallel to the gas flow, which requires further work. Figure 3b and 3c show the formation and dispersion of metal nanoparticles on CNTs after modification. Again, the metal particles are well mixed inside the polymer, particularly for the Ru nanoparticles.

4.2. Gas Permeation Performance of Nanocomposite Membranes. Figure 4 shows the CO_2 and N_2 permeation results of the dense nanocomposite membranes with modified CNTs. The results show that the gas permeation rates observed for most of the nanocomposite membranes are higher than those for pure PES membranes. By addition of nanofillers into the polymer matrix, disturbed polymer chain packing and increased CNT/polymer interfacial volume can be created, which favor gas diffusivity via introducing more alternative routes to pass through gas molecules.³³ The COOH-CNT and Ru-CNT membranes show one common trend that the gas permeation fluxes of both CO_2 and N_2 increase with increasing CNT concentration (<5 wt %). It can be assumed that the free volumes between CNTs and polymer chains are continuous at lower CNT loading (1–5 wt %) leading to lower gas diffusion resistance. However, a higher CNT loading (10 wt %) leads to the CNTs agglomeration or poor dispersion, and it is possible that the created nanogaps between CNTs and polymer chains become uncontinuous and the tortuosity around the aggregated CNTs limits further permeability increment; thus, a slight deterioration of permeation flux is observed at a loading ratio as high as 10 wt %. This phenomenon is matched well with some previous reports.^{30,55} For the Fe-CNT membranes, the permeability keeps increasing even at 10 wt % CNT incorporation, probably due to better dispersion of Fe-CNT at 10 wt % loading. Compared with Ru particles, larger-sized Fe particles derived at higher temperature reduction may obstruct CNT agglomeration and generate more interfacial volume between CNTs and polymer matrix in the composite membranes; therefore, the permeation flux of Fe-CNT membranes goes up even at high CNT concentrations while those of Ru-CNT membranes' counterparts start to

Table 1. Comparison of Permeability and Glass Transition Temperature of Different Modified CNTs–PES Composite Membranes

modifications	max CO ₂ permeation flux (barr)	max CO ₂ permeation enhancement percentage (%)	max CO ₂ /N ₂ selectivity after modification	glass transition temperature (T _g , °C)
pure PES	2.67 ± 0.13	—	21.8	216
COOH-CNT	4.45 ± 0.12	66.7	22.1	221.4 ^a
Ru-CNT	3.56 ± 0.15	33.3	26.5	219.1 ^a
Fe-CNT	4.23 ± 0.09	58.4	12.9	220.3 ^a

^a 5 wt % carbon nanotube incorporation.

decrease because of agglomeration. As a whole, the gas permeability improvement in the nanocomposite membranes is attributed to the disturbed polymer chain packing caused by the addition of nanofillers as reported previously.¹⁷

On the other hand, different gas selectivity can be observed in Figure 4. The gas selectivity of the derived COOH-CNT nanocomposite membranes remains unchanged, compared to pure PES membrane, until the CNT loading ratio reaches 5 wt %. Membranes with Ru-modified CNTs display better performance on both flux and selectivity, while lower selectivity is found in composite membranes with Fe-modified CNTs. The reason may be that the different modifications can cause adsorption difference of gases and consequently affect the gas selectivity of nanocomposite membranes. Larger adsorption differences of N₂ and CO₂ can be introduced by Ru modification than by carboxyl and Fe modification, which will be discussed in the following parts.

The enhancement of gas permeability can be partially governed by the interface between polymer and filler particles. The stiffness of the chain increases, and the forced increase of the interface between polymer and carbon nanotubes may enhance the free volume with increasing T_g from DSC.^{56,57} Table 1 compares the permeability and glass transition temperature of the CNTs–PES nanocomposite membranes. It shows that the glass transition temperature increases with the incorporation of CNTs into the polymer matrix. It is noteworthy that the measured T_g of a pure PES membrane is 216 °C, lower than that reported in some references.⁴⁰ This may be due to the system error resulting from the usage of different PES brands and the instrument for DSC detection. Compared with pure PES membrane, the T_g increases by 3–5 °C after incorporating 5 wt % CNTs into PES matrix. With the disturbed polymer chain packing, the mobility of gas molecules at the molecular level increases, resulting in a permeability increase. A CO₂ permeation flux improvement by 30–70% can be observed around 5 wt % CNT incorporation. When comparing different modified CNTs membranes, COOH-CNT membranes show the highest permeation flux while Ru-CNT membranes show the lowest flux. This result is not in agreement with the glass transition temperature trend, where Ru-CNT sample presents the lowest T_g which indicates a less compact structure for gas permeation, but shows lowest permeability. Therefore, the gas selectivity of composite membranes is mainly influenced by the modification species with different gas adsorption behaviors, rather than polymer chain mobility.

For the CNTs–PES nanocomposite membranes, the Maxwell model (eqs 1 and 3) has been used to simulate the experimental results, as shown in Figure 5. The Maxwell model (eq 1) displays the decrease of permeability, opposite to the experimental results showed above. This non-Maxwell effect has also been observed in

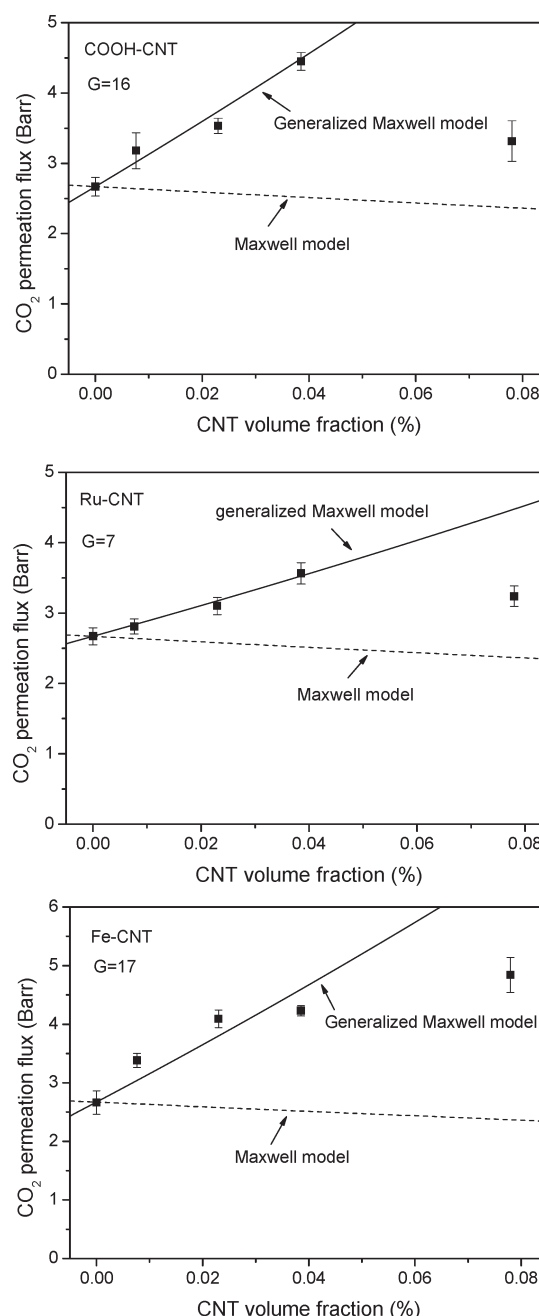


Figure 5. CO₂ permeability through nanocomposite membranes with various modified CNTs.

other polymer–inorganic composite membranes.^{11,13–15,19,21,22} On the other hand, the generalized Maxwell model (eq 3) gives

better predictions of permeation flux especially at low CNT concentrations (<5 wt %). The estimated G parameters of COOH-CNT, Ru-CNT, and Fe-CNT in the generalized Maxwell model are 16 ± 2 , 7 ± 1 , and 17 ± 2 , respectively. The flow obstruction decreases as the G value increases. Therefore, COOH-CNT and Fe-CNT composite membranes, possessing higher G values, present lower gas transport resistance and thus show higher permeation flux than the Ru-CNT modified membrane. These intermediate G values between zero and infinity indicate that the CNT axes are between parallel and vertical to the flow direction due to random dispersion of CNTs in the PES polymer matrix. As an indicator of nanofiller directions in polymer matrix, the G value was originally set to be related to the orientation of the disperse phase. However, the similar dispersions of CNTs in different membranes are observed by TEM images (Figure 3) because the functional groups or metal particles (<5 wt % CNT incorporation) do not alter the random CNT dispersion inside the polymer. Therefore, it can be deduced that the change of G value may be caused by the relationship between adsorption and gas solubility/diffusivity. Combined with the selectivity differences shown in Figure 4 and glass transition temperatures given in Table 1, modification components play a crucial role in selectivity via gas adsorption.

4.3. Effect of Modification Site on Permeability. In order to investigate the gas diffusion route in the modified CNTs–PES nanocomposite membranes, the permeability and selectivity of CNT membrane samples, with Ru nanoparticles deposited on either external or internal wall of nanotubes, were compared. For this purpose, CNTs with different Ru locations were separately prepared with samples denoted as Ru-out-CNT (for external deposition) and Ru-in-CNT (for internal deposition). Figure 6 presents typical TEM images of Ru-in-CNT and Ru-out-CNT. As can be seen in Figure 6, most of the carbon nanotubes in Ru-out-CNT are with closed end while those in Ru-in-CNT are open-ended. Compared to the Ru-out-CNT, the tube length in the Ru-in-CNT is shorter because of the cutting pretreatment to remove the closed end of the CNTs. It is noteworthy that before Ru or Fe doping, Ag has been completely removed from the CNTs by HNO_3 as confirmed by EDS in our previous study.⁵⁸ Examination of Ru positions in these TEM images clearly shows that, for Ru-out-CNT, the Ru particles are mainly deposited on the outer wall of purified nanotubes due to large diffusion resistance in longer and closed tubes. For sample Ru-in-CNT, most of Ru particles are successfully confined into CNT channels. The metal filling efficiency, estimated by visual counting analysis of the location of nanoparticles in TEM, is about 80%. Furthermore, the efficiency of Ru filling was also calculated by analysis of XPS data. As Ru particles confined within the channels of CNTs make no contribution to the XPS signal (the mean free path of excited electrons in graphite (2.6 nm) is shorter than the thickness of the CNTs (~10 nm)), XPS can mainly detect the Ru particles deposited on the outer surface of CNTs. The difference in XPS-detected Ru content and the total Ru loaded on the CNTs can be thereby utilized to calculate the Ru filling efficiency. From the XPS, the Ru metal filling efficiency is around 75% which is consistent with refs 58–60.

Figure 7 shows the permeability of nanocomposite membranes with Ru-out-CNT and Ru-in-CNT. For CNTs with either closed or opened ends employed here, quite surprisingly, the CO_2 permeation fluxes through the two composite membranes are almost identical (~3.55 barrer at 5 wt % CNTs incorporation).

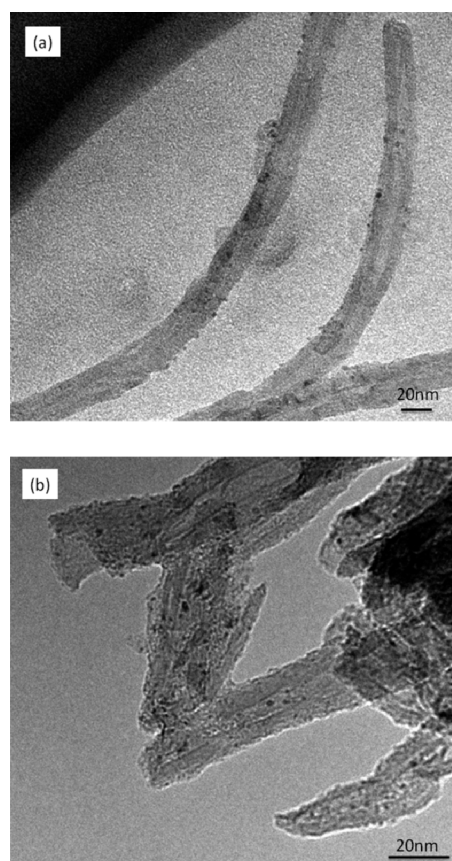


Figure 6. TEM images of Ru-out-CNT (a) and Ru-in-CNT (b) samples.

This may indicate that the gas diffusion path was not through the hollow CNT channels (gas cannot pass through CNT channels with closed caps) but through the interfaces between the nanotubes and polymer chains. On the other hand, a dramatic selectivity difference can be observed by controlling the modification site. Compared to Ru-out-CNT membranes ($\alpha_{\text{CO}_2/\text{N}_2} = 22\text{--}26$), the gas selectivity of membranes with Ru-in-CNT is lower ($\alpha_{\text{CO}_2/\text{N}_2} = 15\text{--}20$). This result illustrates that the Ru particles at different modification sites exhibit different adsorption ability and transport resistance to certain gases like nitrogen. Considering the large thickness of the multiwalled CNTs (7–10 nm), Ru particles inside CNTs may have a negligible effect on gas adsorption properties when gases pass through both free volumes of polymer chains and the nanogaps between the organic–inorganic interface. On the contrary, the modification components on the external surface of CNTs will play a significant role in gas adsorption and diffusivity/solubility behavior, reflected as a change in the permeability.

The selective adsorption of CO_2/N_2 on the modified CNTs is further supported by the density functional calculations. Figure 8 presents the optimized configurations of one N_2/CO_2 molecule adsorbed on the outer surface of CNTs. It is obvious that Fe and Ru are adsorbed at the center of a hexagon on the outer surface of CNTs, while the COOH group is adsorbed on the top of a C atom, which agrees with the reported theoretical results.^{61,62} Figure 9 shows the calculation results of CO_2/N_2 adsorption energy on the inner and outer surface of CNTs modified by either functional groups or metals at the external surfaces. Metals

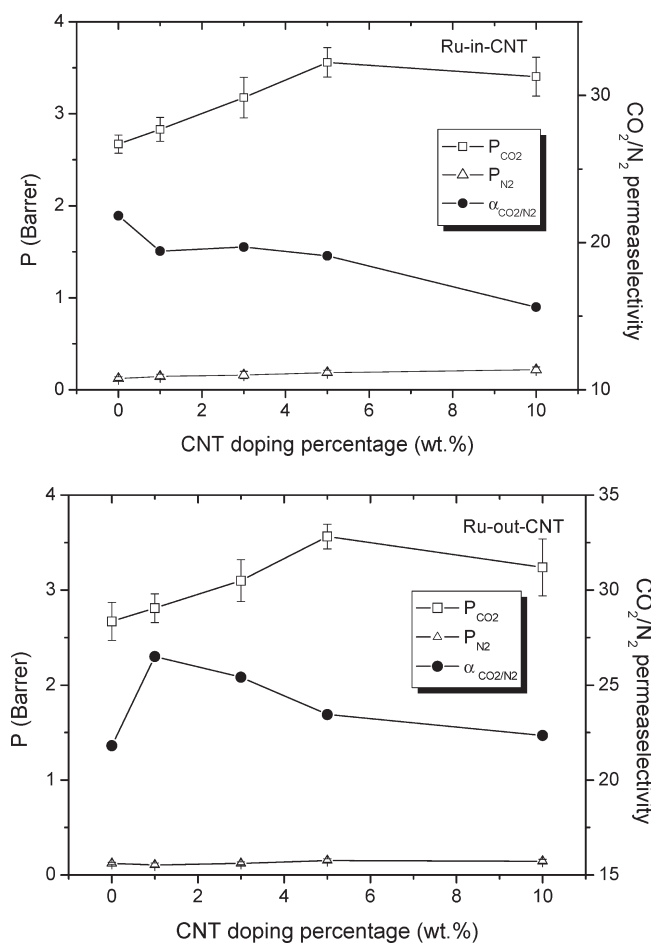


Figure 7. Comparison of permeability of nanocomposite membranes with Ru modified on the external or internal surface of carbon nanotubes.

or functional groups modification on the external surface of CNTs is expected to induce charge transfer between the metals or functional groups and CNTs, thus decreasing the electrostatic potential on the CNT surface, leading to different adsorption of CO_2 and N_2 . The adsorptions of CO_2/N_2 encapsulated in modified CNTs are still physical adsorptions, and the interaction between the gas molecules and CNTs is very weak because of curvature effects of the CNTs. The adsorption energy of inner N_2 and CO_2 on Fe- and Ru-modified CNT channels are similar; thus, the adsorption effect on gas selectivity can be ignored if gas diffusion happens inside the channel and, therefore, the selectivity should be similar for nanocomposite membranes with Fe- and Ru-modified CNTs.

For the adsorption of CO_2/N_2 on the outer surface of Ru-modified CNTs, the strong chemical interaction between the tube and gas molecule occurs due to high chemical reactivity of Ru atom. The distances between Ru atom and O/N atom in CO_2/N_2 are 1.89 and 1.98 Å, respectively. However, the adsorptions of CO_2/N_2 on Fe/COOH modified CNTs are still physical adsorptions, with adsorption energies only a few hundred millielectronvolts. Therefore, the gas adsorption differences between CO_2 and N_2 on the outer surface of modified CNTs are much higher than on the clean CNT surface. Ru-CNT shows the largest adsorption energy difference for CO_2 and N_2 (~0.7 eV), followed by COOH-CNT (~0.27 eV), while Fe-CNT has the

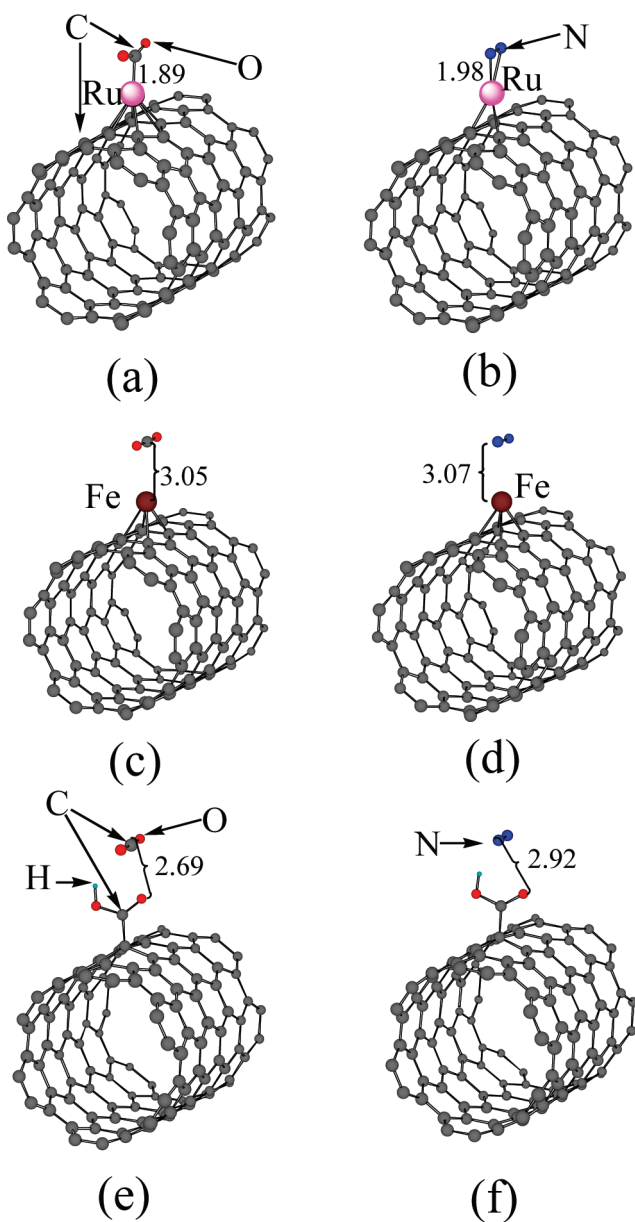


Figure 8. Optimized configurations of (a) CO_2 and (b) N_2 adsorbed on the outer surface of a (6,6) CNT adsorbed with Fe. (c) and (d) are similar to (a) and (b) but with CNTs adsorbed with Ru, (e) and (f) with CNTs adsorbed with COOH.

lowest binding energy difference (~0.07 eV). Large gas adsorption difference, which may change the solubility and total gas selectivity, was introduced via Ru modification. It is noteworthy that although N_2 gas adsorption energy is higher than CO_2 on the external Ru modification sites, the improved CO_2/N_2 selectivity of the composite membranes is observed compared with pure PES membrane. The reason is that CO_2 shows higher transport diffusivity than N_2 for the pure PES membrane. The stronger adsorption of N_2 on modification sites can increase diffusion resistance which generates a negative effect on N_2 gas diffusivity but facilitates the improvement of the total CO_2/N_2 selectivity. Combined with Figure 4 and Table 1, the selectivity variation trends are matched well with the absolute value of the adsorption energy difference. It proves that higher adsorption energy

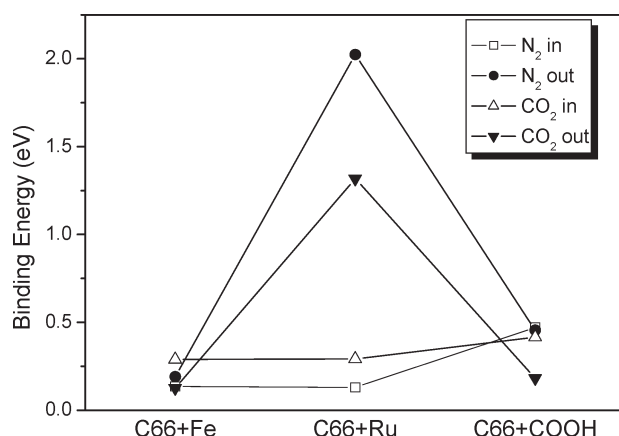


Figure 9. Comparisons of adsorption energies of different gases on CNTs with outer surface modifications.

differences favor gas selectivity improvement. It may be concluded that the gas diffusion mainly occurs in the interface between CNTs and polymer chains in these nanocomposite membranes. The fast diffusion channels of CNTs have not been made use of when they are randomly dispersed in the polymer matrix. The carbon nanotubes mainly act as an impermeable inorganic phase to enlarge the free volume in the polymer matrix, and the gas diffusivity and solubility can be varied by chemical and electrical effects of CNTs. As a whole, the concept of modifying CNTs with functional groups or metal nanoparticles can provide a promising route to improve the selectivity via introducing adsorption differences on active sites when fully aligned carbon nanotubes are used as diffusion tunnels in membranes.

5. CONCLUSIONS

Modified-carbon nanotube/poly(ether sulfone) nanocomposite membranes were prepared and compared in this study. Carboxyl functional groups and Ru and Fe metal particles were used to functionalize the carbon nanotubes for composite membrane fabrication. Based on XRD and TEM results, the crystallinity and morphology of the derived membranes are not altered by introducing functional groups and metal nanoparticles. The gas adsorption variations by modification were investigated by molecular simulation, which revealed that larger CO_2/N_2 adsorption differences were led by Ru modification than by carboxyl and Fe modification. The gas permeation results also show that gas selectivity increases when CNTs are modified by Ru, but remains similar or even decreases when carboxyl and Fe are employed to functionalize CNTs. On the other hand, by controlling the Ru modification site, higher gas selectivity is found when Ru particles are mainly deposited on the external surface of CNTs. Combining and comparing the experimental and modeling results, it can be concluded that gases mainly diffuse through the free volume between the polymer chains and carbon nanotubes in these nanocomposite membranes. The understanding obtained here may lead to the development of a more effective way to further improve composite membrane permeability via external surface modification with inorganic phases that have large gas adsorption differences to various gases.

AUTHOR INFORMATION

Corresponding Author

*E-mail z.zhu@uq.edu.au; fax 61 7 3365 4199.

ACKNOWLEDGMENT

The financial support by the Australian Research Council (ARC) discovery project is greatly appreciated. L.G. also acknowledges the support from IPRS (Endeavour International Postgraduate Research Scholarship, Australia) and UQRS (University of Queensland Research Scholarship).

REFERENCES

- (1) Freeman, B. D.; Pinna, I. *Polymer membranes for gas and vapor separation: chemistry and materials science*; American Chemical Society Meeting, Las Vegas, NV; American Chemical Society: Washington, DC, 1999.
- (2) R. E. Kesting, R. E.; Fritzche, A. K. *Polymeric gas separation membranes*; Wiley: New York, 1993.
- (3) Stern, S. A.; Noble, R. D. *Membrane separations technology: Principles and applications*; Elsevier: Amsterdam, The Netherlands, 1995.
- (4) Park, H. B.; Freeman, B. D.; Zhang, Z.-B.; Sankir, M.; McGrath, J. E. *Angew. Chem., Int. Ed.* **2008**, *47*, 6019–6024.
- (5) Othman, A. M.; Rizk, N. M. H.; El-Shahawi, M. S. *Anal. Chim. Acta* **2004**, *515*, 303–309.
- (6) Zaidi, S.; Matsuura, T. *Polymer membranes for fuel cells*; Springer Verlag: New York, 2009.
- (7) Robeson, L. M. *J. Membr. Sci.* **1991**, *62*, 165–185.
- (8) Robeson, L. M. *Curr. Opin. Solid State Mater. Sci.* **1999**, *4*, 549–552.
- (9) Peng, F.; Lu, L.; Sun, H.; Wang, Y.; Liu, J.; Jiang, Z. *Chem. Mater.* **2005**, *17*, 6790–6796.
- (10) Higuchi, A.; Agatsuma, T.; Uematsu, S.; Kojima, T.; Mizoguchi, K.; Pinna, I.; Nagai, K.; Freeman, B. D. *J. Appl. Polym. Sci.* **2000**, *77*, 529–537.
- (11) Hu, Q.; Marand, E.; Dhingra, S.; Fritsch, D.; Wen, J.; Wilkes, G. *J. Membr. Sci.* **1997**, *135*, 65–79.
- (12) Ismail, A. F.; Rahim, R. A.; Rahman, W. A. W. A. *Sep. Purif. Technol.* **2008**, *63*, 200–206.
- (13) Joly, C.; Goizet, S.; Schrotter, J. C.; Sanchez, J.; Escoubes, M. *J. Membr. Sci.* **1997**, *130*, 63–74.
- (14) Joly, C.; Smahi, M.; Porcar, L.; Noble, R. D. *Chem. Mater.* **1999**, *11*, 2331–2338.
- (15) Kim, J. H.; Lee, Y. M. *J. Membr. Sci.* **2001**, *193*, 209–225.
- (16) Li, Y.; Chung, T.-S.; Cao, C.; Kulprathipanja, S. *J. Membr. Sci.* **2005**, *260*, 45–55.
- (17) Merkel, T. C.; Freeman, B. D.; Spontak, R. J.; He, Z.; Pinna, I.; Meakin, P.; Hill, A. J. *Science* **2002**, *296*, 519–522.
- (18) Moaddel, M.; Koros, W. J. *J. Membr. Sci.* **1997**, *125*, 143–163.
- (19) Peng, F.; Lu, L.; Sun, H.; Wang, Y.; Liu, J.; Jiang, Z. *Chem. Mater.* **2005**, *17*, 6790–6796.
- (20) Tantekin-Ersolmaz, S. B.; Atalay-Oral, C.; Tatller, M.; Erdem-Senatalar, A.; Schoenau, B.; Sterte, J. *J. Membr. Sci.* **2000**, *175*, 285–288.
- (21) Tena, A.; Fernandez, L.; Sanchez, M.; Palacio, L.; Lozano, A. E.; Hernandez, A.; Pradanos, P. *Chem. Eng. Sci.* **2010**, *65*, 2227–2235.
- (22) Winberg, P.; DeSitter, K.; Dotremont, C.; Mullens, S.; Vankelecom, I. F. J.; Maurer, F. H. *J. Macromolecules* **2005**, *38*, 3776–3782.
- (23) Gong, T.; Zhang, Y.; Liu, W. J.; Wei, J. Q.; Jia, Y.; Wang, K. L.; Wu, D. H.; Zhong, M. L. *Mater. Lett.* **2008**, *62*, 4431–4433.
- (24) Qian, D.; Dickey, E. C.; Andrews, R.; Rantell, T. *Appl. Phys. Lett.* **2000**, *76*, 2868–2870.
- (25) Song, L.; Zhang, H.; Zhang, Z.; Xie, S. S. *Composites, Part A* **2007**, *38*, 388–392.
- (26) Ackerman, D. M.; Skoulios, A. I.; Sholl, D. S.; Johnson, J. K. *Mol. Simul.* **2003**, *29*, 677–684.

- (27) Skouidas, A. I.; Ackerman, D. M.; Johnson, J. K.; Sholl, D. S. *Phys. Rev. Lett.* **2002**, *89*, 185901.
- (28) Skouidas, A. I.; Sholl, D. S.; Johnson, J. K. *J. Chem. Phys.* **2006**, *124*, 054708.
- (29) Kim, S.; Pechar, T. W.; Marand, E. *Desalination* **2006**, *192*, 330–339.
- (30) Cong, H. L.; Zhang, J. M.; Radosz, M.; Shen, Y. Q. *J. Membr. Sci.* **2007**, *294*, 178–185.
- (31) Weng, T.-H.; Tseng, H.-H.; Wey, M.-Y. *Int. J. Hydrogen Energy* **2009**, *34*, 8707–8715.
- (32) Cong, H.; Radosz, M.; Towler, B. F.; Shen, Y. *Sep. Purif. Technol.* **2007**, *55*, 281–291.
- (33) Ismail, A. F.; Goh, P. S.; Sanip, S. M.; Aziz, M. *Sep. Purif. Technol.* **2009**, *70*, 12–26.
- (34) Zhu, Z. H.; Lu, G. Q.; Smith, S. C. *Carbon* **2004**, *42*, 2509–2514.
- (35) Du, A. J.; et al. *Nanotechnology* **2009**, *20*, 375701.
- (36) Neogi, P. *Diffusion in polymers*; CRC Press: Boca Raton, FL, 1996.
- (37) Maxwell, J. *A treatise on electricity and magnetism*; Clarendon Press: Oxford, England, 1873.
- (38) Toy, L. G.; Freeman, B. D.; Spontak, R. J.; Morisato, A.; Pinna, I. *Macromolecules* **1997**, *30*, 4766–4769.
- (39) Yu, M.; Funke, H. H.; Falconer, J. L.; Noble, R. D. *Nano Lett.* **2009**, *9*, 225–229.
- (40) Chiou, J. S.; Maeda, Y.; Paul, D. R. *J. Appl. Polym. Sci.* **1987**, *33*, 1823–1828.
- (41) Liu, J.; Rinzler, A. G.; Dai, H.; Hafner, J. H.; Bradley, R. K.; Boul, P. J.; Lu, A.; Iverson, T.; Shelimov, K.; Huffman, C. B.; Rodriguez-Macias, F.; Shon, Y.-S.; Lee, T. R.; Colbert, D. T.; Smalley, R. E. *Science* **1998**, *280*, 1253–1256.
- (42) Balasubramanian, K.; Burghard, M. *Small* **2005**, *1*, 180–192.
- (43) Banerjee, S.; Hemraj-Benny, T.; Wong, S. S. *Adv. Mater.* **2005**, *17*, 17–29.
- (44) Wang, C.; Guo, S.; Pan, X.; Chen, W.; Bao, X. *J. Mater. Chem.* **2008**, *18*, 5782–5786.
- (45) Ordejón, P.; Artacho, E.; Soler, J.; Soler, M. *Phys. Rev. B* **1996**, *53*, R10441.
- (46) Sánchez-Portal, D.; Ordejón, P.; Artacho, E.; Soler, J. M. *Int. J. Quantum Chem.* **1997**, *65*, 453–461.
- (47) Troullier, N.; Martins, J.; Luriaas *Phys. Rev. B* **1991**, *43*, 1993–2006.
- (48) Kleinman, L.; Bylander, D. M. *Phys. Rev. Lett.* **1982**, *48*, 1425–1428.
- (49) Perdew, J. P.; Zunger, A. *Phys. Rev. B* **1981**, *23*, 5048–5079.
- (50) Monkhorst, H. J.; Pack, J. D. *Phys. Rev. B* **1976**, *13*, 5188–5192.
- (51) Khulbe, K. C.; Matsuura, T.; Lamarche, G.; Lamarche, A. M. *J. Membr. Sci.* **2000**, *170*, 81–89.
- (52) Chowdhury, G.; Kruczak, B.; Matsuura, T. *Polyphenylene oxide and modified polyphenylene oxide membranes: Gas, vapor, and liquid separation*; Kluwer Academic Publishers: Dordrecht, The Netherlands, 2001.
- (53) Guan, R.; Zou, H.; Lu, D.; Gong, C.; Liu, Y. *Eur. Polym. J.* **2005**, *41*, 1554–1560.
- (54) Khayet, M.; García-Payo, M. C. *Desalination* **2009**, *245*, 494–500.
- (55) Kim, S.; Chen, L.; Johnson, J. K.; Marand, E. *J. Membr. Sci.* **2007**, *294*, 147–158.
- (56) Bartoš, J. *Colloid Polym. Sci.* **1996**, *274*, 14–19.
- (57) Sharma, S. C.; Mandelkern, L.; Stehling, F. C. *J. Polym. Sci., Part B: Polym. Lett.* **1972**, *10*, 345–356.
- (58) Wang, L.; Ge, L.; Rufford, T. E.; Chen, J. L.; Zhou, W.; Zhu, Z. H.; Rudolph, V. A. *Carbon* **2011**, *49*, 2022–2032.
- (59) Pan, X.; Bao, X. *Chem. Commun.* **2008**, 6271–6281.
- (60) Pan, X.; Fan, Z.; Chen, W.; Ding, Y.; Luo, H.; Bao, X. *Nat. Mater.* **2007**, *6*, 507–511.
- (61) Fagan, S. B.; Mota, R.; da Silva, A. J. R.; Fazzio, A. *Physica B* **2003**, *340*–*342*, 982–985.
- (62) Wang, C.; Zhou, G.; Liu, H.; Wu, J.; Qiu, Y.; Gu, B.-L.; Duan, W. *J. Phys. Chem. B* **2006**, *110*, 10266–10271.